Electronic Supplementary Material (ESI) for Catalysis Science & Technology.

Supporting information

Electropolymerized Metal-Protoporphyrin electrodes for Selective Electrochemical Reduction of CO_2

Nael G Yasri,[1] *Tareq A. Al-Attas*,[1] *Jinguang Hu,*[1]* *Md Golam Kibria*[1]*

Department of Chemical and Petroleum Engineering, Schulich School of Engineering, University of Calgary, 2500 University Drive NW, Calgary, Alberta T2N 1N4, Canada

Correspondence: md.kibria@ucalgary.ca, Jinguang.hu@ucalgary.ca

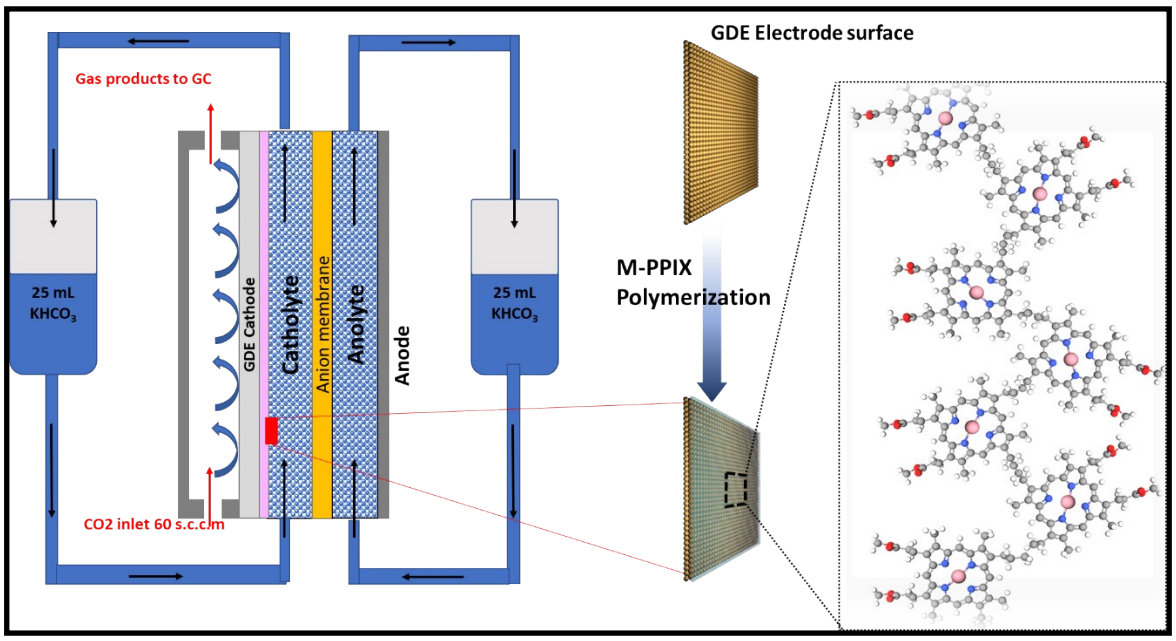

Figure [SI 1]: Schematic of the three-compartment flow electrolyzers used in this work for CO_2RR, ilusterating the cathodic side of the gas-diffusion electrode (GDE) modified by metal-protoporphyrin particles.

Table [SI 1]: Different organo metallic/porphyrin catalysts for electrocatalytic CO_2RR

Catalyst	Potential (V vs RHE)	*j* (mA cm^{-2})	FE (%)	Main Products (FE)	Electrolyte	Ref.
PorCu[1]	-0.976	49	59	CH_4(27%), C_2H_4 (17%), CO (10%)	0.5M $KHCO_3$	[1]
Cu-Pc[2]	-1.6	N/A	~50	CH_4 (30%), CO, HCOOH	0.5M $KHCO_3$	[2]
Fe-Por/ NR[3]	−0.79 V	0.71 mA cm^{-2}	92.1%	CO	0.1 M KCl	[3]
Fe– Por/MOF [4]	0.6	-1	91%	CO	0.5M $KHCO_3$	[4]
Fe-Por	-1.16 (V vs NHE)	0.31	94	CO	*DMF/H2O/Et NCO_2CH_3/NB u_4PF_6	[5]
3D-FePGH [5]	−0.49 V	0.42 mA cm^{-2} (partial for CO)	96.4%	CO	0.1 M $KHCO_3$	[6]
SAML M-Por [6] (Fe or Co)	-1.6 V vs. Ag/AgCl	N/A	5-30% CO and HCOOH	HCOOH (Fe), CO (Co)	0.1 M $NaHCO_3$	[7]
COF-Co-Por	-0.67	3.2	91	CO	0.5M $KHCO_3$	[8]
COF-Co@CNT [7]	-0.68	40	94	CO	0.5 M KHCO3	[9]
Co-Por@CNT [8]	–0.65	5.2 (CO)	90%	CO	0.5 M NaHCO3	[10]
Cu_2O/Cu	-1	3	~62	CH_4 (7%), C_2H_4 (12%), CO, HCOOH	0.1M KCl	[11]
Cu– Por/MOF [9]	−0.7 V	3.2	44.3%	HCOOH	0.5 M $KHCO_3$	[12]
2D Cu-Por/MOF [10]	−1.55 V vs. Ag/AgCl	4.5	85.2	CH_3COOH CHOOH	** CH_3CN/H_2O/ $EMIMBF_4$	[13]
Cu nanoparticles	-1.35	12	76	CH_4	0.1M $NaHCO_3$	[14]
Cu-Por/GMC [11]	- 1.278	13	40% (C_2H_4 max)	CO, CH_4, C_2H_4	0.1 M KCl	[15]
Reduced Cu_2O film	-0.55	2.6	75	CO (40%), HCOOH (33%)	0.5M $NaHCO_3$	[16]

[1]Cu-Por: is Cu- Prophorin, [2] Cu-Pc: is Cu- phthalocyanine, [3] Fe-Por/ NR: Fe Porphyrin nanoreactor, [4] Fe– Por/MOF: Fe–Porphyrin- Based Metal–Organic Framework, [5] 3D-FePGH is three-dimensional porphyrin/graphene hydrogel, COF-Co-Por: covalent organic frameworks (COF) comprising Co porphyrin, [6] SAML-M-Por: Self-Assembled Monolayers of Metal Porphyrins, [7] COF-Co@CNT: covalent organic frameworks (COF) comprising Co porphyrin on carbon nanotubs, [8] Co-Por@CNT: Co porphyrin on carbon nanotubs, [9] Cu– Por/MOF: Cu–Porphyrin-MOF Based Metal–Organic Framework, [10] 2D Cu-Por/MOF: copper porphyrin metal–organic framework nanosheets, [11] Cu-Por/GMC: Molecular Cu-Complex Immobilized on Graphitized Mesoporous Carbon.

* 0.4M $EtNCO_2CH_3$ + 0.1M NBu_4PF_6 in DMF + 2M H_2O

** CH_3CN solution with 1 M H_2O and 0.5 M ionic liquid 1-ethyl-3-methylimidazolium tetrafluoroborate ($EMIMBF_4$)

SI. 1. EXPERIMENTAL

SI. 1. 1. Materials and Catalyst Preparation

Reagent-grade chemicals were purchased from Sigma-Aldrich Scientific and used as received. Metalation of protoporphyrin IX dimethyl ester (MW = 590.71 g mol^{-1}, Sigma Aldrich) was performed according to the method described by Adler at al.[17] Briefly, 100 mmol of protoporphyrin IX dimethyl ester (59 mg) was reflected in 50mL of N,N '-dimethylformamide (99.9% reagent grade) in a 200 mL volume two-neck round bottle flask. Following the complete dissolution, a stoichiometric amount of the corresponding metal ions (100 mmol of either cobalt acetate or copper acetate) is added and the reaction is allowed to proceed. The completion of the metal exchange is checked by the loss of the free porphyrin's red fluorescence under long-wave UV light (or spectrophotometrically, SI. 2 and Figure [SI2]).

Following metalation, the reaction flask was cooled in an ice-water bath for 15 min, then 50 mL of chilled distilled water is added and the resulting partially crystalline precipitate is filtered on a pre-weighed filter, washed with water, dried and calculate the yield (97%). The prepared metalloporphyrin (Cu-PPIX and Co-PPIX) then used to modify the gas diffusion electrodes (GDEs), polymerized and compared with the metal-free porphyrin for electrochemical and material characterization as well as CO_2RR performance. The characterization and the electrochemical performance were achieved on either of a glassy carbon (GC) or gas diffusion electrode (GDE).

Electrochemical polymerization of metalloprotoporphyrin on glassy carbon electrode (GC; 3 mm diameter, CH-Instruments, Inc.) was performed in a 10-mL volume three-electrode system cell with GC electrode, Ag/AgCl (3 M KCl), and Pt wire as working, reference, and counter electrode, respectively. The electrolyte of methylenechloride and 0.1M of TBAP contained 10 mmol of metalloprotoporphyrin (M-PPIX) at an applied voltage window of 0.0-1.2 V vs Ag/AgCl electrode for the indicated number of cycles at a scan rate of 50 mV/s.

The modification of the GDEs with Cu-PPIX and Co-PPIX was performed via spray coating followed by electrochemical polymerization. The catalyst (8 mg) was dispersed in a volumetric mixture of 2:6:0.4 (mL) of water : isopropyl alcohol (99.8%, Sigma-Aldrich) : Nafion (perfluorinated resin solution, 5 wt. % in a mixture of lower aliphatic alcohols and water, contains

45% water, Sigma-Aldrich). The purpose of using the Nafion solution is to uniformly disperse the catalyst and to act as a binder onto the GDE surface. The mixture was sonicated for one hour and then spray coated via a nitrogen gun (Nozzle diameter 0.1mm) on top of the carbon paper (80 cm^2) with a uniform catalyst loading at 0.1 mg/cm^2. The electrochemical polymerization of the coated protoporphyrin on GDE was performed according to a modified method described by Macor and Spiro [18]. Briefly, a 6 x 2 cm GDE that was already spray-coated with the electroactive metalloprotoporphyrin was connected to the potentiostat as a working electrode, conjugated with a counter electrode (10 cm long platinum wire, diameter 0.25 mm, Sigma-Aldrich) and Ag/AgCl (sat. KCl, 0.197 V vs SHE) reference electrode in a three-cell electrodes system. The electro-polymerization was performed in 80 mL methylene-chloride and 0.1M of tetrabutylammonium perchlorate (TBAP) as an electrolyte at an applied voltage of 1.2 V vs Ag/AgCl electrode for 15 min. For successful polymerization, care should be given that the spray-coated electrode will not be kept in the electrolyte before applying a potential to prevent monomer dissolution.

The prepared metalloprotoporphyrin and the electropolymerized films were then characterized via Raman spectroscopy (WiTec Alpha-300 series microscope utilizing a 532 nm diode laser excitation). Soft X-ray absorption spectroscopy (sXAS) at the Co *L*-edge, Cu *L*-edge, and N *K*-edge were performed at the spherical grating monochromator (SGM) beamline 11ID-1 at the Canadian Light Source (CLS) synchrotron. All measurements were performed at room temperature using Amptek silicon drift detectors (SDDs) in the fluorescence yield mode with an energy resolution of approximately 120 eV. Each sample was scanned five times, where the scanning time was 1 min. The spot of sample measurement moved by 0.1 mm between each measurement to eliminate the possibility of radiation damage on the sample. The sample was mounted at an angle of roughly 45° with respect to both the detectors and the incident beam. The beam spot size was focused to approximately 50 μm by microscopy using Kirkpatrick-Baez mirror system. The Co *L*-edge was scanned between 950 and 1150 eV, while the Cu *L*-edge was scanned between 950 and 1150 eV, the N *K*-edge was scanned between 380 and 430 eV.

The surface morphology of the prepared metalloprotoporphyrin and their electropolymerized form were studied by scanning electron microscopy (SEM-EDS) (Phenom proX Desktop). UV–Vis spectra of protoporphyrin free base and the prepared metalloprotoporphyrins dispersed in water were obtained using a spectrophotometer (Lambda 25, PerkinElmer).

Measurement of the electrochemically active catalyst in the polymerized Co-PPIX and Cu-PPIX films formed on GC electrodes were estimated based on the plot of the peak current of the oxidation waves produced by Co^{I} /Co^{II} and Cu^{I}/Cu^{II} in the respective voltammograms. The amount of the corresponded electroactive species on the electrode surface determined according to the Faraday's Law using the following equation:

$$\Gamma = \frac{Q}{nFA}$$

where Γ is the electroactive amounts of metal-complex in the formed film, Q (coulombs) is the total charge determined by integrating the area under the oxidation peak, n is the number of electrons consumed, F is the Faraday constant (96485 C mol^{-1}), and A is the electrode area (7 mm^2).

SI. 1. 2. Electrolysis for CO_2RR on GDE

To demonstrate the potential use of the prepared GDE in electrochemical CO_2RR in aqueous media we used a three-compartment electrochemical flow cell of anolyte, catholyte, and gas chambers (Figure SI 1). The catholyte and the anolyte chambers are separated via anion-exchange membrane (Fumapem FAB-PK-130), whereas, the catholyte and the gas chambers are separated via GDE as a working electrode. Both catholyte and the anolyte chambers have thicknesses of ca. 15 mm. The three-electrode system employed are; the prepared working electrode of GDE coated with the catalyst (the exposed surface area is 1 cm^2), the reference electrode of Ag/AgCl (3.5 M KCl saturated with silver chloride, CH Instruments, Inc.), and the counter electrode made of nickel foam (1 cm^2 long, 1.6 mm thickness, 350 g/m^2 surface density, MTI Corporation). The three-electrode system was monitored via a potentiostat (Bio-Logic potentiostat, SP-300) applying a chronoamperometry mode. Identical electrolytes of 20 mL volume of 1.0 M $KHCO_3$, 20 mL each, was continuously circulated through the anolyte and the catholyte chambers at a flow rate of 50 ml/min during the electrochemical reaction using peristaltic pumps (Mini-Pump Variable Flow; 0.4 to 85 mL/min, Cole-Parmer Peristaltic Pump) with silicone tubing (Shore A: 50 Versilic® PST-50). The applied potentials were converted from Ag/AgCl scale to the conventional reversible hydrogen electrode (RHE) scale applying Nernst equation: $E_{RHE} = E_{Ag/AgCl\,(3.5\,M\,KCl)} + 0.059 \times pH + 0.205$. The flowrate of CO_2 (Air Liquide, 99.999%) was kept steady at 60 s.c.c.m, and the experiments were performed at ambient temperature and pressure.

SI. 1. 3. CO_2RR products analysis and calculation

Analysis of the CO_2RR products was performed for gas outlet. The gas products of the CO_2 reduction, i.e., H_2, CO, CH_4, and C_2H_4 were analyzed by gas chromatography (PerkinElmer Clarus 680) equipped with a flame ionization detector (FID) and a thermal conductivity detector (TCD) and using argon (Air Liquide, 99.999%) as a carrier gas. The Faradaic efficiency of the gas products was evaluated using the following equation:

$$FE_x(\%) = \frac{i_x}{i_{total}} \times 100 = \frac{n_x\, v_{gas}\, c_x\, F}{i_{total}\, V_m} \times 100$$

where i_x is the partial current for the indicated product (x), i_{total} is the current density measured during the reaction, n_x number of electrons transferred to produce 1 mole of x, v_{gas} is the flow rate of CO_2, c_x is the concentration of the product x detected by the GC, F is Faraday constant (96,485 Coulomb/mol) and V_m represents the unit molar volume of gaseous at Standard Laboratory Conditions (SLC) (298.15 K and 100 KPa), which is 24.5 L/mol.

The turnover frequency (TOF) was calculated as follows:

$$TOF_x(s^{-1}) = \frac{i\ (A\ cm^{-2}) \times FE_x(\%)}{n_x \times F\ (C\ mol^{-1}) \times N_{tot}(mol)}$$

where i is the current density, FE_x is the Faradaic efficiency of the product of interest, F is the Faraday constant, N_{tot} is the total moles of catalyst used during the electrolytic reaction.

SI. 2. Spectroscopic investigtion on the metal inseartion into the PPIX bocket

The UV-Vis spectra of the original PPIX-H_2 in DMF (black line, Figure SI 2) shows a Soret band transition (B band) at 405 nm and the other three lower intensity Q bands located at 504, 539, and 575 nm. These bands are all originated from π–π* transitions [19]. The changes in the absorption spectra of Co-PPIX (blue line) and Cu-PPIX (red line), when compared to the original PPIX-H_2, can be considered as an evidence of metals insertion into the "pocket" of the porphyrin ligand. Both metal complexes exhibited Q bands at positions differe from those of the origin PPIX-H_2 (i.e. at 507, 543 and 556 nm for Co-PPIX, and at 534, and 570 nm for Cu-PPIX). Although the UV-visible spectra provide little information regarding the saturation of the central porphyrin ligand,

together with the information obtains from XAS spectra can prove quite definitive information about the metalation products of protoporphyrin.

The Raman spectra obtained from the prepared Co-PPIX, Cu-PPIX, and their film formed on GC electrodes are shown in Figure [SI 4], and the typical Raman shifts are listed in Table [SI 2]. The original PPIX-H_2 sample is sensitive to the Raman input wavelength (532 nm) which coincides with an absorption band of the sample wherein the relaxation pathway generates heat and resulted in sample damage with no resolved spectra reported. However, both Co-PPIX and Cu-PPIX produce well defined similar spectra with shifts in bands that are known to be strongly affected by the type of both metal and ligand (i.e. the direct charge-transfer interactions between the *d* orbitals on the metal and the inductive effects produced by the ligands).[20] For example, the antisymmetric stretching of C-NH-C that is red-shifted in Co-PPIX (1336 cm^{-1}) as compared with Cu-PPIX (1365 cm^{-1}) due to the higher electron withdrawal by Co that is reflected on the stretching energy of the ligands.[21]

It has been well established that Raman spectra of molecules in the polymerized state exhibit bands between 50 and 400 cm^{-1} due to the vibration of molecules about their position in the lattice.[22] These vibrations are known as Translation vibrations (along the axes of molecules), Liberation vibration, and the combined Translation/Liberation vibrations [23]. The frequency of such vibration is low because the mass of molecules is large and the intermolecular elastic forces are small (see the spectra of polymerized molecules in Figure [SI 4] at wave number range 100-500 cm^{-1}). The interpretation of these bands is out of the scope of this work and gives no additional information about the structure characterization other than confirming the formation of a polymerized type of film on the electrode.

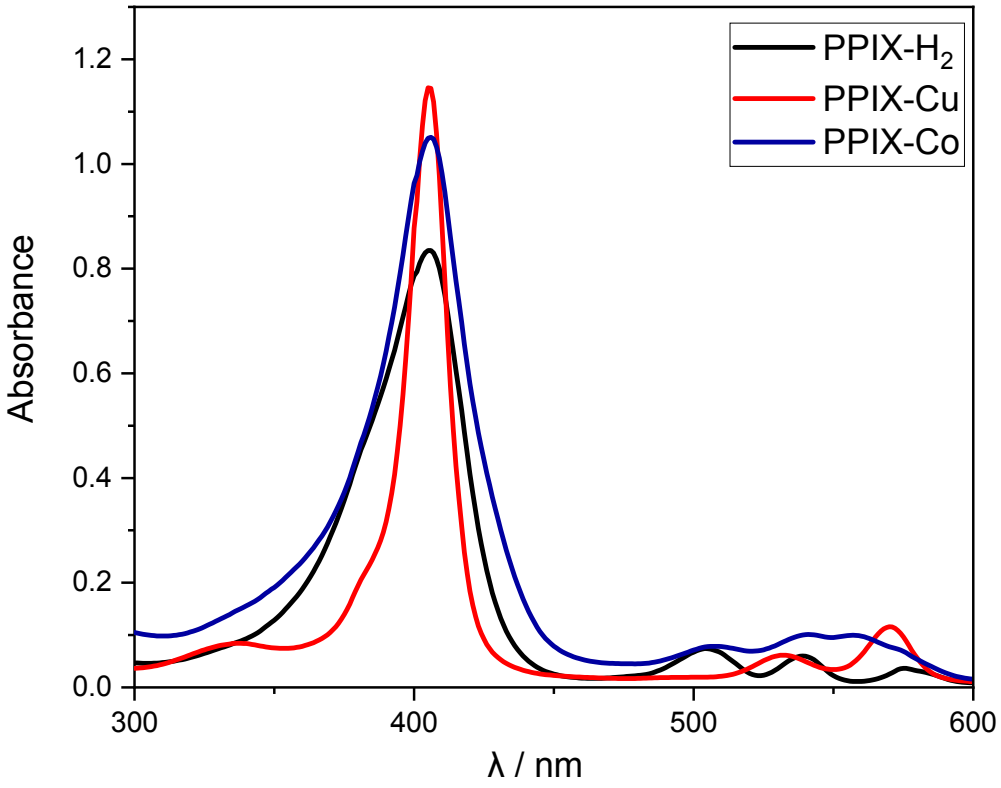

Figure [SI 2]: UV-Visible spectra of the as prepared Co-PPIX and Cu-PPIX compared with the original PPIX-H_2 in DMF solution.

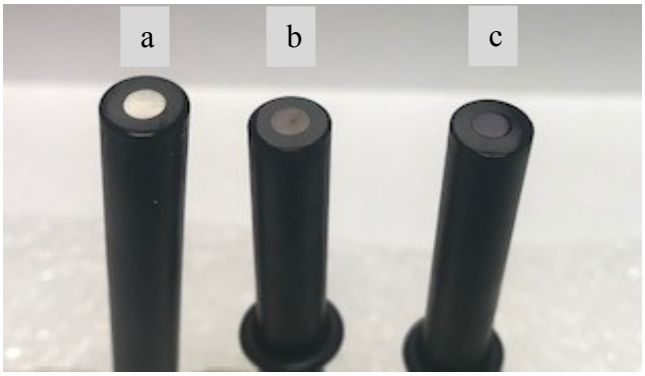

Figure [SI 3]: images of a clean GC electrode (a) and the electropolemrised films of Co-PPIX (b) and Cu-PPIX (c) on GC electrodes.

SI. 3. Raman spectra of the spray coated and polymerized catalysts on GDEs

Both the D- and G-bands appeared with sort of noises on the spectra (Orange lines), with that the center of both the D- and G-bands exhibited blue shifts of about 14.3 cm^{-1} in D-band and 12.3 cm^{-1} in G-band for the Co-PPIX complex, and about 10.6 cm^{-1} in D-band and 6.4 cm^{-1} in G-band for the Cu-PPIX complex. The disruptiveness of both D- and G-bands after polymerization may be due to the interference with the other bands that belong to the added polymer molecules. Although the common investigation of Raman spectra for carbonaceous structure always focuses on the intensity of bands, in this study it is difficult to evaluate those bands due to the coincide of the graphitic backbone with those of metal-PPIX complexes bands. Moreover, the blue shifts of both the D-band and G-band are signs of structural stress on the backbone carbon skeletons induced via the introduction of heterogeneous atoms[24, 25] and the type of charge carriers on the surface,[24, 26] respectively. In this case, the introduction of polymeric molecules, as well as the oxidative reactions that occur during polymerization, may result in inducing the structurer compression in the carbon bonding of the backbone structure of GDE and thus resulting in the appearance shifts of the D-bands. Considering the shifts in the G-Bands, however, they have been assigned in the literature for the modification of the charge carrier concentration at the surface.[24] Meaning that when a heterogeneous doping of backbone carbon introduces holes to the structure a redshift will occur, whereas, blueshift always associated with the introduction of electrons.[26] The Raman blue shifts of the G-bands of the polymerized GDE indicating the rises in the surface's charge-carrier-density due to the introduction of metal complexes of PPIX. Moreover, in addition to the G- and D-bands, the spectra show bands between 100 and 600 cm^{-1} that are not well resolved. Compare these bands with the corresponding Raman spectra of the polymerized Co-PPIX or Cu-PPIX on GC electrode (see the red spectra in Figure [SI 4] for comparison) we can predict that the bands between 100-600 cm^{-1} are associated with the polymerized molecules on GDE, which can be an evidence of the successful polymerization of the corresponded molecules on GDE.

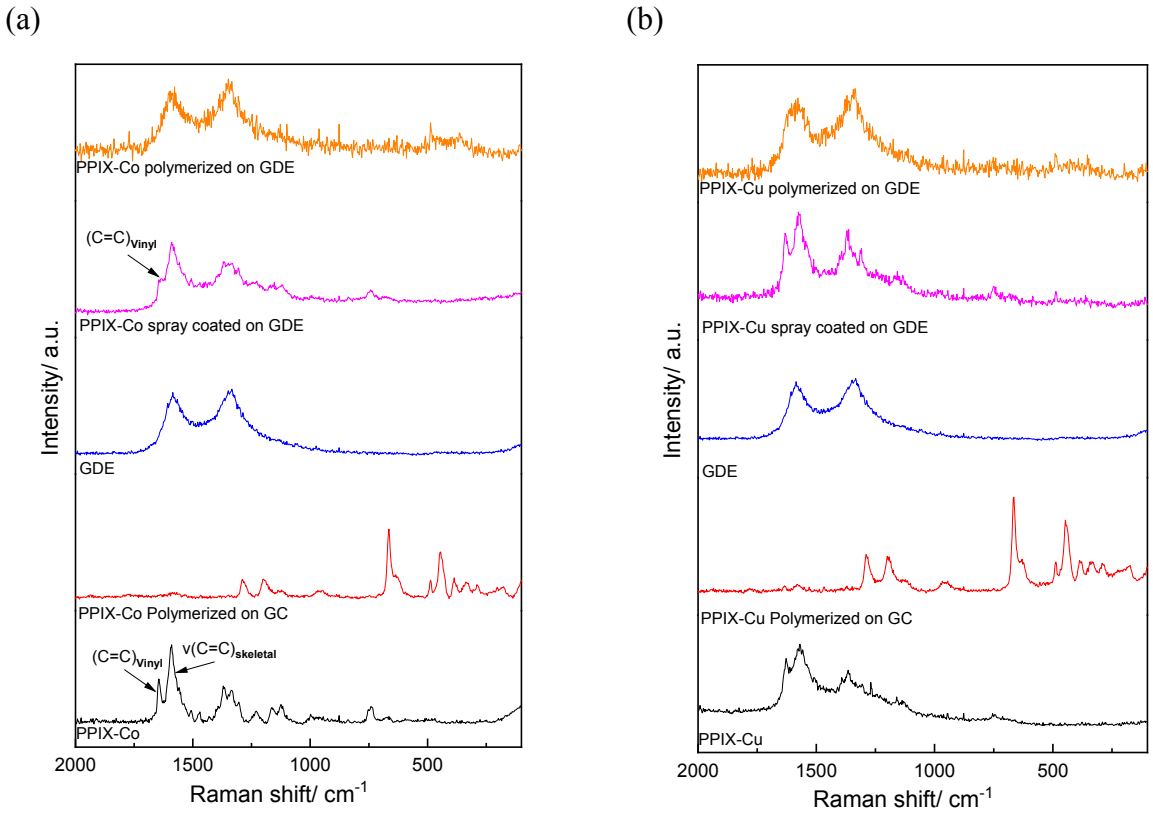

Figure [SI 4]: Raman spectra of; a) Co-PPIX and b) Cu-PPIX at different preparation stages of GC and GDE electrodes. The spectra are all normalized to the post edge levels.

SI. 4. Discussion on SGM results

The XAS spectra of the spray-coated monomers and the electropolymerized complexes on electrodes exhibited absorption bands coincide with the same energy bands of the corresponding metals species. Figure [SI 5] shows the Co $L_{2,3}$-edge of the prepared cobalt catalysts (a), and Cu $L_{2,3}$-edge of the prepared copper catalysts (b) at different preparation stages along with spectra obtained from Co (II) oxide and Cu (II) oxide standards. The spectra are all normalized to the post edge levels. The L_2-edge and L_3-edge are pronounced $2p^{1/2}$-3d and $2p^{3/2}$-3d transitions. The shape of the spectra can be used to investigate the change occur to the electronic structure of metal species when complexed with the linker and depending on the functional group presented. The central energy for Co L_2 and L_3 edges in CoO (II) appears at 781.3 eV and 767.4 eV, respectively;

whereas, for Cu L_2 and L_3 edges in CuO (II) is 939.2 eV and 919.9 eV, respectively. Insertion of Co and Cu species to complex with PPIX molecules produce a similar profile of their corresponded metal oxides spectra, which provides clear evidence of the successful complexation of both Co and Cu species with PPIX (Note that the free metals will be washed out during the metal-PPIX filtration). Moreover, the *L*-edge of the metal-PPIX complex is shifted to higher energy with respect to the non-porphyrin. The value of these shifts is equal to 0.5 eV for both of Co-L_3 edge and Cu-L_3 edge, and equal to 0.3 eV for both of Co-L_2 edge and Cu-L_2 edge in the PPIX complexes. According to Baker *et al.* [27] who studied Heme molecules (Fe-centered porphyrin), these shifts are due to strong σ donation in the porphyrin like molecules that shifting the hybridized bonding in the ligand to higher energy. Comparing the profiles of the spectra obtained from both Co-PPIX and Cu-PPIX with spectra observe in the literature when introducing inductive effects from a square planar nitrogen linker ligands on cobalt[28] and copper[29, 30] sites, confirmed an increased electron density with a slight shift in the energy towered higher values.[29] Moreover, careful observation of the Co-PPIX spectra, the low energy feature in the L_3-edge (absorptions at ~765.0 eV and 766.8 eV) can be assigned as being associated with a dπ transition (i.e. filling the dπ* hole) and it is unlike the higher energy-intense L_3 peak (767.4 eV) which is dominantly σ donor character. Comparing with the Cu species which inherently has full outer shell 3d orbitals it lacks the low energy spectral feature. Considering on the other hand the adsorption bands of the spray-coated Co-PPIX (767.4, and 781.3 eV) and Cu-PPIX (919.9 and 939.2 eV), they both appear at the same energy with the corresponding monomeric metal-PPIX, which indicates no inductive effects of GDE on the centered metal in the monomers.[31]

Furthermore, the N *K*-edge XAS spectrum of the as prepared Co-PPIX and Cu-PPIX exhibits the typical strong signals in both π* (394.5 and 395.7 eV) and σ* (409.4 eV) bands (Figure [SI 10]). The peak (a) at 395.7 eV correspond to the pyridinic structure, the peak (b) at 395.7 eV the pyrrolic structure, and the peak at 409.4 eV is due to C–N σ* transitions.[31] These peaks are almost appeared at the same position to the corresponding metal-PPIX spray coated and polymerized on GDE, but widen the π* bands, indicating of the interaction of the π-π hybridization in the carbon structure with the N-metal bonding.[32, 33] However, no shift in position of both π* and σ* bands would indicate no changes in the metal-N matrix structure and the metal still cadged within the porphyrin framework.[31]

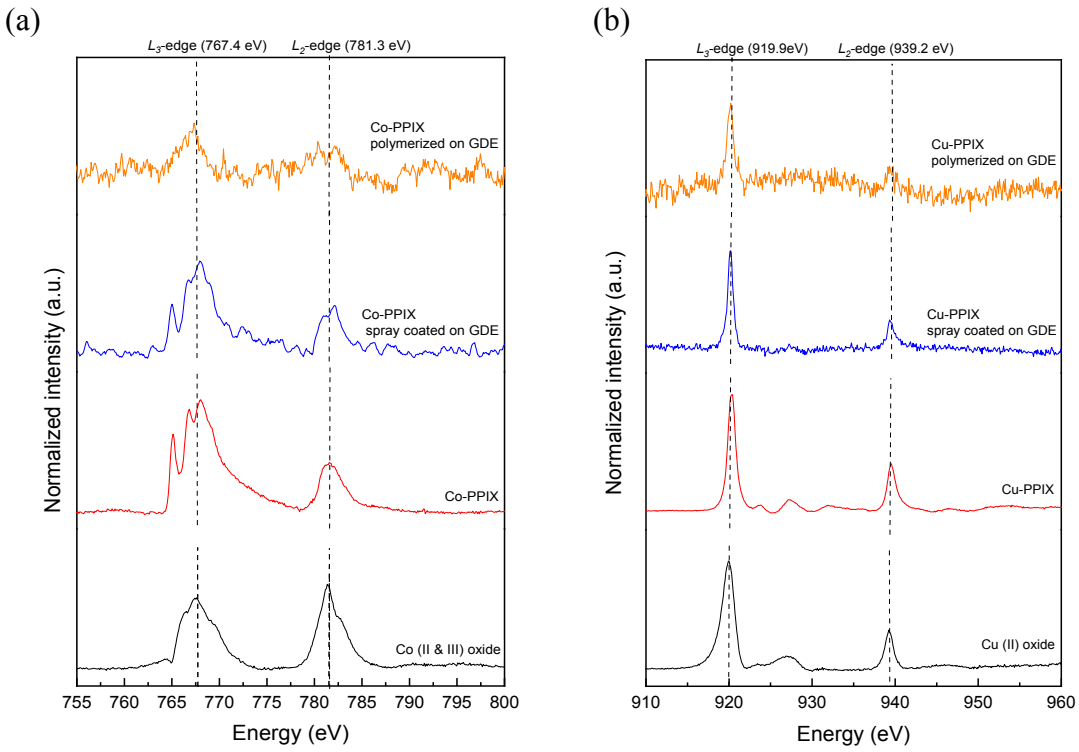

Figure [SI 5]: (a) The Co $L_{2,3}$-edge of the prepared cobalt catalysts, and (b) Cu $L_{2,3}$-edge of the prepared copper catalysts along with spectra obtained from Co (II) oxide and Cu (II) oxide standards. The spectra are all normalized to the post edge levels.

Table [SI 2]: Raman band assignments of Co-PPIX and Cu-PPIX (references [34-36]				
Vibrational assignment *	Raman shift (cm^{-1})			
	Co-PPIX	Co-PPIX polymerized	Cu-PPIX	Cu-PPIX polymerized
ρ (C-C-N)	--	664	--	664
δ (C-N-C)	743	--	754	--
ν (Pyrrole breath)	998	Split 949 & 974	967	Split 946 & 969
δ (C-H), (C-C)	1124	1122	1127	1114
δ (C-N)	1165	1137	1160	Shoulder
ν (C-NH-C)	1303	1289	1306	1289
ν_a (C-NH-C)	1336	--	1365	--
τ (H-C-C-C)	1370	--	1389	--
ν(C=C) skeletal	1592	1568	1568	1580
ν(C=C) Vinyl	1642	--	1627	1635
*** Vibration symbol; δ = Bending, ν = stretching, ρ = rocking, ω = wagging, τ = twisting, ν_a = antisymmetric stretching**				

SI. 5. Electrochemical film formation on GC electrode from Co-PPIX:

The use of oxidative scan in the voltammogram has been thoroughly investigated for the formation of films of various metallo-protoporphyrin (i.e. Zn, Co, Ni, Cr, Fe, and Mn) on electrodes from various electrolytes and different applications.[37, 38] During the electro-polymerization of

protoporphyrin, Synder and White[39] reported that degradative oxidation can occur on protoporphyrin molecules at a potential higher than the potential responsible for vinyl group's saturation for polymer formation (0.9 V_{SCE}). Thus, a careful choice for the value of the applied potential will be required to avoid the degradative oxidation during the electro-polymerization of a protoporphyrin film on an electrode (ca. 1.4 V_{SCE}).

The first CV exhibits two redox peaks at formal potentials of $E_{1/2}$ = 0.74 and $E_{1/2}$ = 0.94 $V_{Ag/AgCl}$ with peak-to-peak separation values higher than 0.57 mV indicating slow electron transfer processes (i.e. irreversible electrochemical redox reactions with ΔE_1 = 0.125 V and ΔE_2 = 0.118 V). Increasing the number of scans result in a dramatic increase in the oxidative waives, whereas the reduction waves increased in the negative direction only in the first 15 cycles and then produces identical reduction waves. Increasing the cycle number will increase the values of peak-to-peak separation of the redox processes (see Figure [SI 6, b] for ΔE_1,), which indicates an increase in the irreversibility of the electron exchange for the grown film. Moreover, monitoring the increases in the oxidative peak currents, although both of the oxidative peaks are simultaneously increased, the trend of Δj (j_{a2}-j_{a1}) with increasing the cycle number indicates that the increase of current in the oxidative scans are associated more with first peak (i.e. j_{a1}) [ref]. The trend of Δj (j_{a2}-j_{a1}) shows a plateau between cycle 3-10 then decreased dramatically, which indicates that the process responsible for j_{a1} is more dominant after 10 cycles then the process corresponds to j_{a2}.

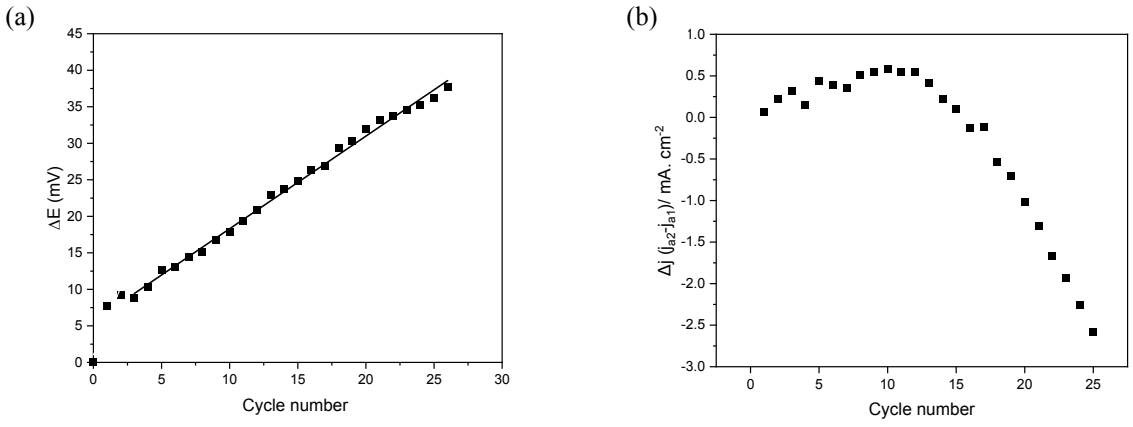

Figure [SI 6]: successive oxidative cycle voltammograms of GC electrode in DCM/0.1M TBAP

as an electrolyte and 10 mmol of a) Co-PPIX and b) Cu-PPIX. The scan rate 50 mV s^{-1}. c) the values of peak-to-peak separation for the redox processes of Co-PPIX electrochemical filme formation on GC electrode with increasing the cycle number, and d) the trand of Δj (j_{a2}-j_{a1}) with increasing the cycle number during the electropolymerisation of Co-PPIX. The electrolyte is methylenechloride and 0.1M of TBAP contained 10 mmol of metalloprotoporphyrin at an applied voltage window of 0.0-1.2 V vs Ag/AgCl for the indicated number of cycles at a scan rate of 50 mV/s.

SI. 6. Evaluating the electrochemically active catalysts formed on the GC electrod

The amount of electrochemically active catalysts formed on the GC electrode was determined according to the Faraday's law of electrolysis using the oxidative waves observed in the voltammograms for Co(I)/Co(II) and Cu(I)/Cu(II) (see inset Figure [SI 7, a-b]).[40] The calculated values from both electrodes found almost similar, i.e. 12.5×10^{-10} mol cm^{-2} for Co-PPIX film and 13.5×10^{-10} mol cm^{-2} for Cu-PPIX film, which indicate that the film formation on GC electrode using M-PPIX is featured by the structure ligand of their molecules and not depend on the type of metal center. Comparing these results with Co-phthalocyanine complex immobilized onto chemically converted graphene (14×10^{-10} mol cm^{-2}),[40] our results show similar electrochemically active catalysts despite our condition of using smooth GC surface (low defect) and their use of highly defected graphene to provide an ideal surface for immobilization. These compared results provide more shreds of evidence on the poor interaction between the stacked molecules on graphene and the electrode when a conventional coating is applied. Electro-polymerization in this case links the catalyst molecules at the electrode surface to enhance the electron exchange capability.

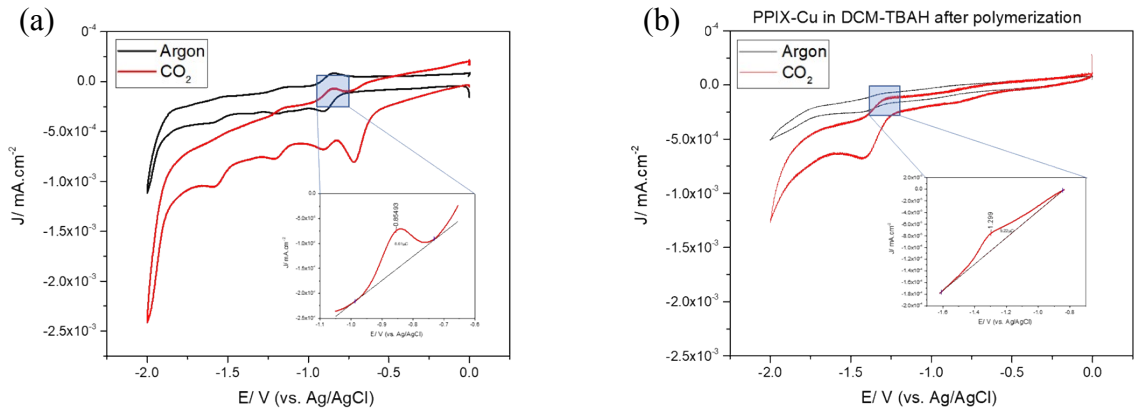

Figure [SI 7]: Reductive cyclic voltammograms of the monomeric form of a) Co-PPIX and b) Cu-PPIX in 0.1M TBAP/DCM solutions saturated with Ar (black line) and with CO2 (red line). The reductive cyclic voltammograms of the polymerized films of c) Co-PPIX and d) Cu-PPIX using the same electrolyte. The CVs scanned between +0.0 V and -2.0 V vs Ag/AgCl, at a scan rate 50 mV s^{-1}.

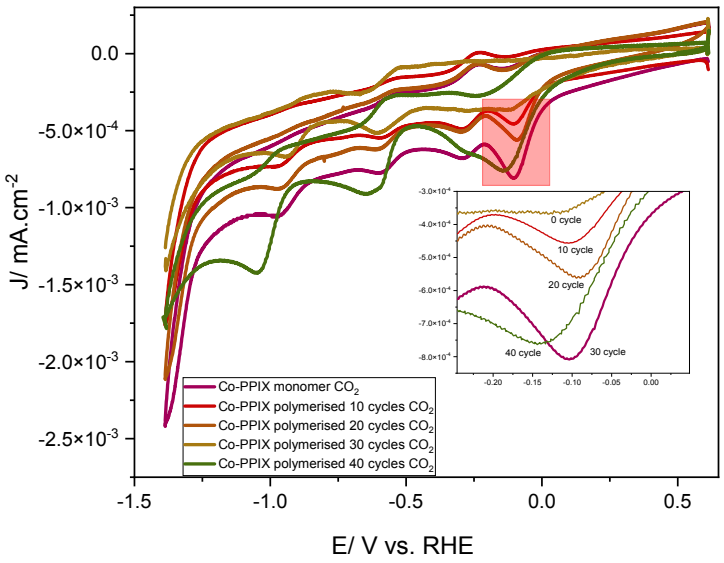

Figure [SI 8]: Reductive cyclic voltammograms of the Co-PPIX catalyst in 0.1M TBAP/DCM solutions saturated with CO_2 after oxidative CVs between 0 and 40 cycles. The CVs scanned between +0.0 V and -2.0 V vs Ag/AgCl, at a scan rate 50 mV s^{-1}. Inset shows enlarge view of peaks in the range 0.0 to -0.2 V_{RHE}.

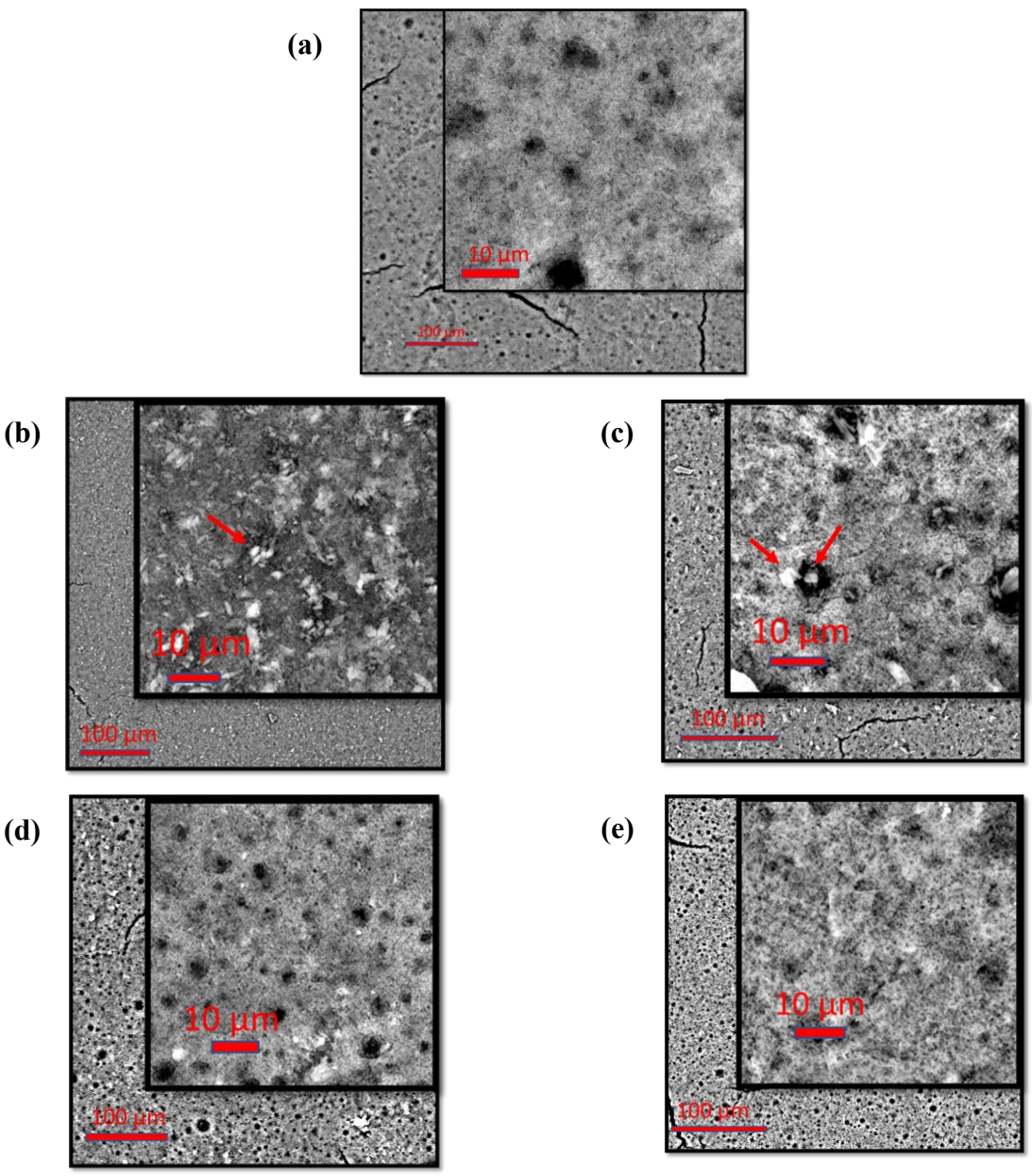

Figure [SI 9]: Scan Electrone Microscop images of; a) GDE, b), Cu-PPIX spray coated on GDE, c) Co-PPIX spray coated on GDE, d) electropolymerized Cu-PPIX after spray coating on GDE, and e) electropolymerized Co-PPIX after spray coating on GDE.

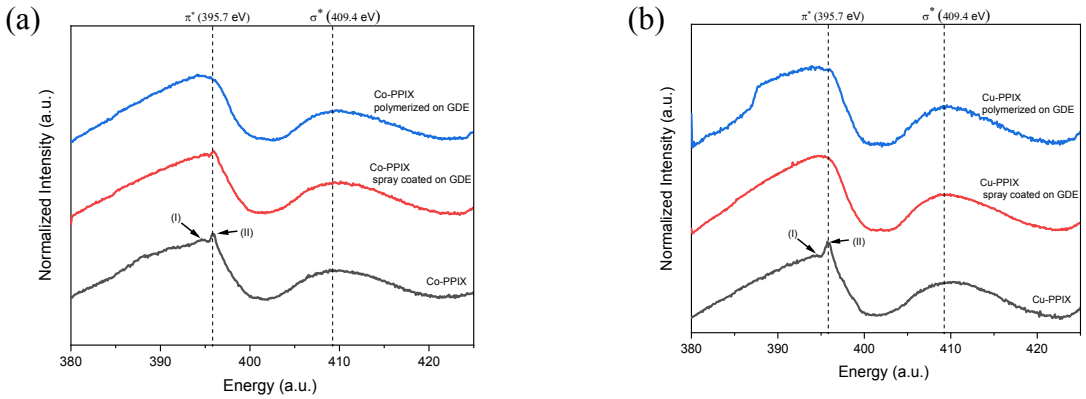

Figure [SI 10]: the N *K*-edge of c) Co-PPIX, and b) Cu-PPIX at different preparation stages on GDE electrodes.

SI. 7. Linear Sweep Voltammetry investigation of the GDE electrode:

Remarkably, when the flowing gas is CO_2, the linear sweep voltammograms (LSVs) of the modified GDEs exhibit lower onset potentials and slightly higher cathodic currents as compared with the argon flowing gas within the potential window tested (from 0.5 to -1.0 V_{RHE}) (Figure [SI 8, a and b]), which is an indication of the higher electrochemical catalytical activity toward CO_2. For instance, flowing CO_2 gas, an onset potential of about 0.49 V_{RHE} was observed with both Co-PPIX polymerized (green curve) and unpolymerized films (red curve), whereas, with the argon flowing gas this type of onset potential was not obtained (only onset potentials for HER appear at -0.6 V_{RHE}) (Figure [SI 11, a]). On the other hand, the Cu-PPIX films show different LSV behavior as compared with the Co-PPIX films (Figure [SI 11, b]). The Co-PPIX films exhibit in the presence of CO_2, current shoulders of about -2.0, and 0.84 Acm^{-2} at a potential of 0.0 V_{RHE} for the polymerized and unpolymerized films, respectively. Whereas, the Cu-PPIX films show with CO_2, less pronounce current peaks at 0.45 V_{RHE} and shoulders at about -0.32 V_{RHE} (see inset, Figure 4b). These current peaks and shoulders may be associated with the adsorption of CO_2 on the catalysts and dissociation of its reaction products, respectively. The same peaks and shoulders do not appear when the reaction media is argon.

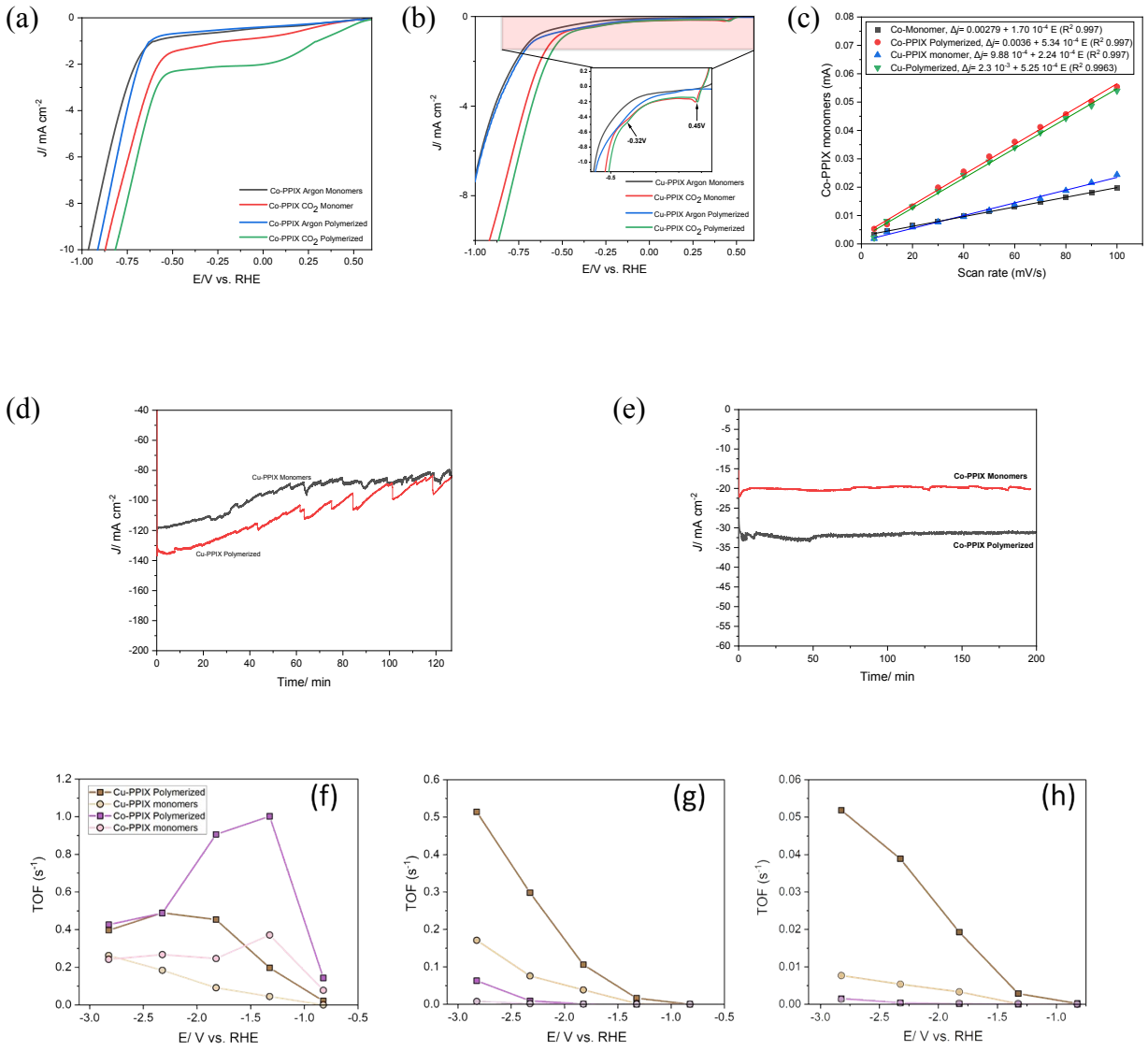

Figure [SI 11]: a & b) respective LSVs for Cu-PPIX and Co-PPIX containing electrode in the presence of CO_2 or argon as flowing gases in a flow-type electrolyzer. c) the liner plots of the CV scan rate vs. the capacitive currents $\Delta j=(j_{anodic}-j_{cathodic})$ of the prepared GDE electrodes of Cu-PPIX and Co-PPIX in the monomeric and polymeric forms. To ensur the resulting current is not Faradaic, the CV windows for the Cu-PPIX containing electrodes performed from 0.48 to -0.58 V_{RHE} and for the Co-PPIX containing electrodes performed from 0.78 to 0.88 V_{RHE}. d & e) current density recorded during the stability test with Cu-PPIX and Co-PPIX containing electrode in the presence of CO_2 as flowing gases in a flow-type electrolyzer. f, g, f) the turnover frequency (TOF) for the productions of; f) CO, g) CH_4, and h) C_2H_4 at different potentials using Co-PPIX and Cu-PPIX both in the polymerized and monomeric forms..The electrolyte in the flow cell electrolyzer is 1M $KHCO_3$ and the flow rate of the gases is 60 s.c.c.m.

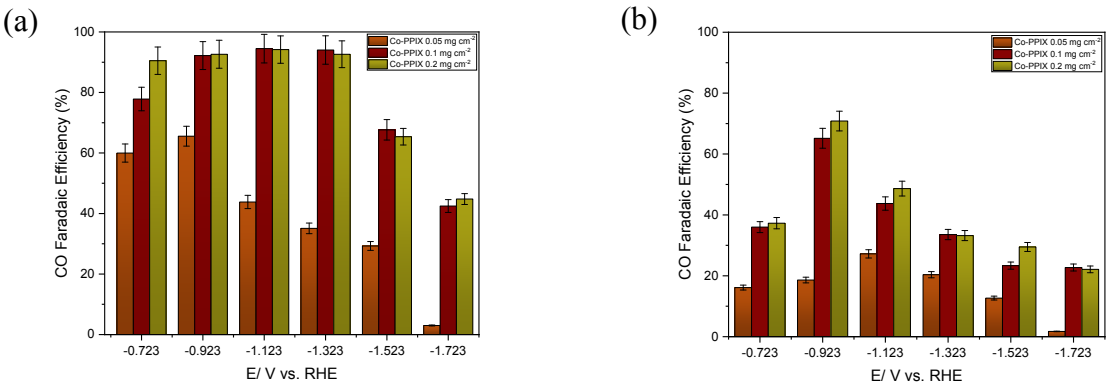

Figure [SI 12]: Faradaic efficiencies for the production of CO at different potentials using; a) polymerized Co-PPIX, and b) the monomeric Co-PPIX at different loading.

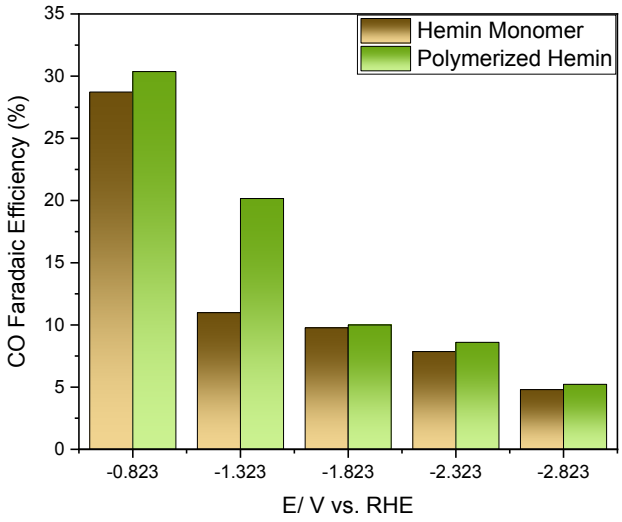

Figure [SI 13]: Faradaic efficiencies for the production of CO at different potentials using Hemin in a monomeric and polymeric form at different potential.

Characterization of the catalysts after CO_2RR

To investigate the structural change of the catalysts after CO_2RR, we characterized the dissembled electrodes following 2 hours CO_2RR via XAS and UV-Vis spectroscopies (See Figure [SI 14] for a flow chart of the characterization experiments). The use of XAS spectra to assist the change in the structure has been employed to investigate the electronic structure of catalysts.[41] The XAS spectra of the spent catalysts (monomer and polymer after CO_2RR) are shown in Figure SI 15. The spectra clearly show strong L_2 and L_3 absorption edges, and no substantial shape differences before and after CO_2RR, indicting no substantial changes in the chemical structures during CO_2RR. For instance, in the Co-containing catalysts, the L_2 and L_3-edges, as well as, the low energy feature near the L_3-edge (absorptions at 776.6 eV) still appear in the monomeric structure of the spent Co-PPIX catalyst. Moreover, the polymerized catalyst still lacks the low energy spectral feature, which is attributed to the high electron delocalization in the polymer structure (See the above XAS section; "*Discussion on SGM results*" and Figure [SI 5] for comparison). In general, the separation between L_3- and L_2-edges has been used in the literature to indicate changes in the oxidation state of the coordinated metal of the catalyst. [42, 43] In the case of Co-PPIX (Figure [SI 14a]), both the monomeric and the polymeric forms show similar L_3-L_2 splitting values. These are 14.82 eV for the monomer and 14.92 eV for the polymer before reactions (measured from Figure [SI 5a]), which maintain at similar values of 14.74 eV, and 15.06 eV in the spent catalysts, respectively. Thus, the level of L_3-L_2 splitting, as well as the similarity of the spectra before and after electrolysis (of the same preparation), can indicate no change in the Co state during electrolysis. Considering on the other hand the Cu-PPIX catalysts, the energy separation between L_3- and L_2-edges is dependent on the oxidation state of Cu (19.0 eV for Cu (II) and 21.0 eV for Cu (I)).[43] The monomeric and the polymeric forms of Cu-PPIX show a similar value of 19.3 eV for the L_3-L_2 splitting that increased to 20.3 and 20.2 eV in the spent monomer and polymer catalysts, respectively. These L_3-L_2 splitting increased from the ideal value of Cu (II) (19 eV), but still lower than the separation value of Cu (I) (21.0 eV). These increases maybe related to the delocalization of the electrons on the porphyrin ligand or maybe the presence of mixed Cu (II) and Cu(I) form after electolysis.[43]

The UV-Vis spectra of the spray-coated metal-free PPIX-H_2 on GDE before and after polymerization was collected using DMF solution and compared with the spectra of the similarly treated metal-based M-PPIX (see Figure SI 14). The B-band along with the Q-bands of the metal-

free PPIX-H_2 of the monomeric (Figure SI 14b,c) and the polymeric structures (Figure SI 14e,f) show different behavior to those of the metal-based catalysts (M-PPIX). However, the M-PPIX spectra before and after CO_2RR show similar patterns that can be considered as evidence of a low probability of the conjugated metal ions to reduce to the metallic forms during CO_2RR. For example, the spectrum of the monomer PPIX-H_2 (Figure SI 14c-d) shows 4 Q bands at 504, 539, 578, and 630 nm, whereas, the spray-coated monomer before and after CO_2RR exhibited only 2 Q-bands (at 540 and 573 nm with the Co-PPIX, and 531, and 570 nm with the Cu-PPIX catalysts, respectively). The disappearance of the Q-bands at 404 and 630 nm combined with blue-shifts of the remaining peaks in the M-PPIX (freshly prepared and spent catalysts) can be considered as spectroscopic evidence of the conjugated π- electrons in the porphyrin structures with the metal cations.[1] Considering the polymerized catalysts (Figure SI 14e,f), however, the metal-free PPIX-H_2 exhibited a wide B-band (centered at about 397 nm) that is red-shifted as compared with the PPIX-H_2 monomer. This broadening and red shifting suggest that an increase in the electron delocalization throughout the backbone structure of the formed polymer [44]. The Q-bands of the polymerized PPIX-H_2 also showing different shapes compare to those of the monomer, metallic, and the spent polymerized M-PPIX forms. Whereas, the spectra of the freshly polymerized M-PPIX and spent catalysts showing both similar behavior, indicating that the optical properties were not altered during the electrocatalytic reaction and that the integrity of the metal cation into the porphyrin unit was confirmed during CO_2RR. Further investigation of the metal (Co and Cu) hybridization structures can be studied using various approaches (e.g. XPS spectroscopy, C^{13} NMR, or field emission spectroscopy), however, our UV-Vis and XAS investigations along with results found in the literature,[1, 45] prove no demetallation or metal cation reduction of the M-PPIX during CO_2RR.

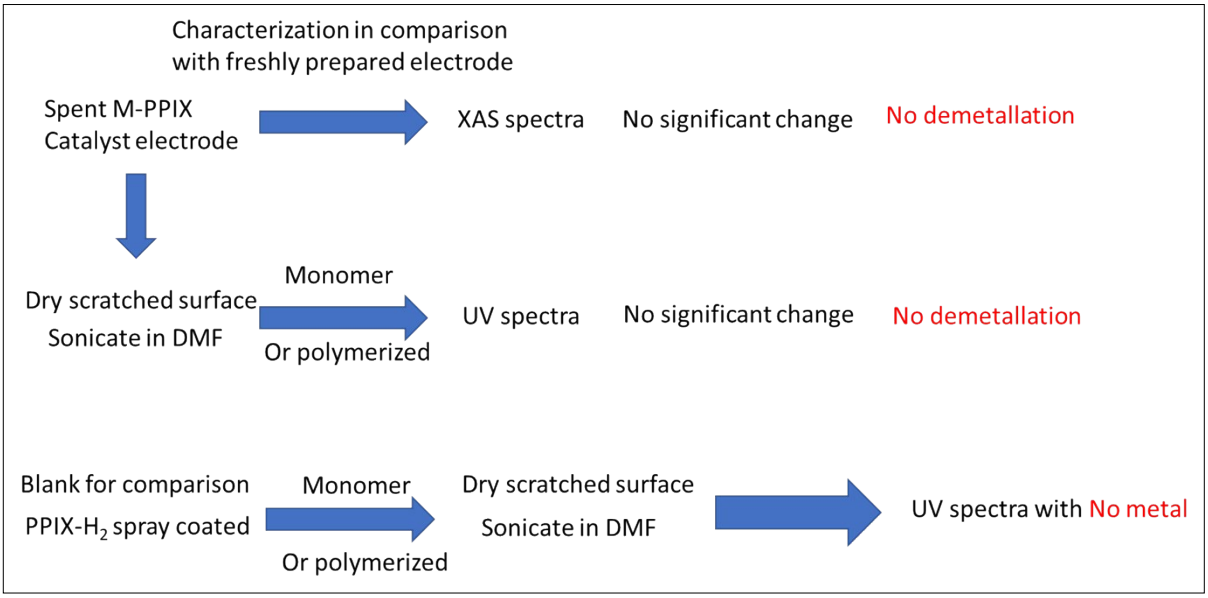

Figure [SI 14]: A flow chart of the set of control experiments performed to investigate the reduction of metal cations in M-PPIX to metals.

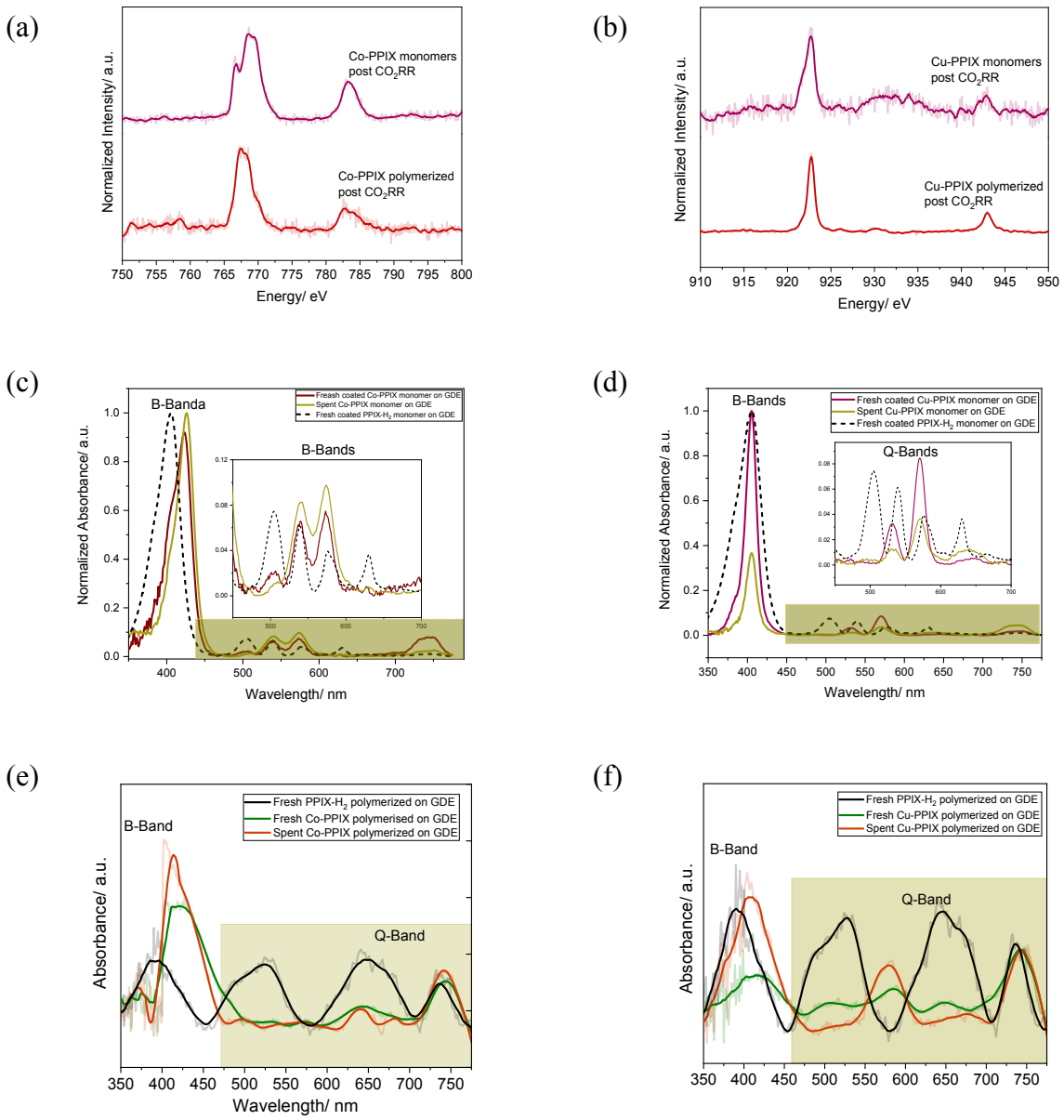

Figure [SI 15]: The $L_{2,3}$-edge of the spent monomeric and polymeric cobalt catalysts of (a) Co-PPIX, (b) Cu-PPIX. The spectra are all normalized to the post edge levels. (c-f) the UV-Vis spectra of (c) the freshly prepared and spent Co-PPIX catalysts in the monomeric form, d) the freshly prepared and spent Cu-PPIX catalysts in the monomeric form, e) the freshly polymerized and spent Co-PPIX catalysts in the polymeric form, and e) the freshly polymerized and spent Co-PPIX catalysts in the polymeric form.

References

1. Z. Weng, J. Jiang, Y. Wu, Z. Wu, X. Guo, K. L. Materna, W. Liu, V. S. Batista, G. W. Brudvig and H. Wang, *JACS*, 2016, **138**, 8076-8079.
2. R. Matheu, E. Gutierrez-Puebla, M. Á. Monge, C. S. Diercks, J. Kang, M. S. Prévot, X. Pei, N. Hanikel, B. Zhang, P. Yang and O. M. Yaghi, *JACS*, 2019, **141**, 17081-17085.
3. J. Choi, J. Kim, P. Wagner, J. Na, G. G. Wallace, D. L. Officer and Y. Yamauchi, *Journal of Materials Chemistry A*, 2020, **8**, 14966-14974.
4. B.-X. Dong, S.-L. Qian, F.-Y. Bu, Y.-C. Wu, L.-G. Feng, Y.-L. Teng, W.-L. Liu and Z.-W. Li, *ACS Appl. Energy Mater.*, 2018, **1**, 4662-4669.
5. C. Costentin, S. Drouet, M. Robert and J.-M. Savéant, 2012, **338**, 90-94.
6. J. Choi, J. Kim, P. Wagner, S. Gambhir, R. Jalili, S. Byun, S. Sayyar, Y. M. Lee, D. R. MacFarlane, G. G. J. E. Wallace and E. Science, 2019, **12**, 747-755.
7. J. A. Mennel, H. Pan, S. W. Palladino and C. J. Barile, *The Journal of Physical Chemistry C*, 2020, **124**, 19716-19724.
8. S. Lin, C. S. Diercks, Y.-B. Zhang, N. Kornienko, E. M. Nichols, Y. Zhao, A. R. Paris, D. Kim, P. Yang, O. M. Yaghi and C. J. Chang, *Science*, 2015, **349**, 1208-1213.
9. Y. Lu, J. Zhang, W. Wei, D.-D. Ma, X.-T. Wu and Q.-L. Zhu, *ACS Applied Materials & Interfaces*, 2020, **12**, 37986-37992.
10. M. Zhu, J. Chen, L. Huang, R. Ye, J. Xu and Y.-F. Han, *Angew. Chem. Int. Ed.* , 2019, **58**, 6595-6599.
11. S. Lee, D. Kim and J. Lee, 2015, **54**, 14701-14705.
12. M.-J. Liu, S.-M. Cao, B.-Q. Feng, B.-X. Dong, Y.-X. Ding, Q.-H. Zheng, Y.-L. Teng, Z.-W. Li, W.-L. Liu and L.-G. J. D. T. Feng, *Dalton Trans.*, 2020, **49**, 14995-15001.
13. J.-X. Wu, S.-Z. Hou, X.-D. Zhang, M. Xu, H.-F. Yang, P.-S. Cao and Z.-Y. Gu, *Chem. Sci.*, 2019, **10**, 2199-2205.
14. K. Manthiram, B. J. Beberwyck and A. P. Alivisatos, *JACS*, 2014, **136**, 13319-13325.
15. M. Balamurugan, H.-Y. Jeong, V. S. K. Choutipalli, J. S. Hong, H. Seo, N. Saravanan, J. H. Jang, K.-G. Lee, Y. H. Lee, S. W. Im, V. Subramanian, S. H. Kim and K. T. Nam, 2020, **16**, 2000955.
16. C. W. Li and M. W. Kanan, *JACS*, 2012, **134**, 7231-7234.
17. A. D. J. J. I. N. Adler, Chem., *J Inorg Nucl Chem.*, 1970, **32**, 2443-2445.
18. K. Macor and T. J. J. o. t. A. C. S. Spiro, *JACS*, 1983, **105**, 5601-5607.
19. J. Patwari, A. Chatterjee, S. Sardar, P. Lemmens and S. K. Pal, *Phys. Chem. Chem. Phys.*, 2018, **20**, 10418-10429.
20. M. Hanana, H. Arcostanzo, P. K. Das, M. Bouget, S. Le Gac, H. Okuno, R. Cornut, B. Jousselme, V. Dorcet and B. J. N. J. o. C. Boitrel, 2018, **42**, 19749-19754.
21. D. R. Roy, E. V. Shah and S. Mondal Roy, *Spectrochim. Acta A Mol. Biomol. Spectrosc.*, 2018, **190**, 121-128.
22. J. J. Kim, J. McLeish, A. J. Hyde and R. T. Bailey, *Chem. Phys. Lett.*, 1973, **22**, 503-506.
23. D. J. J. o. R. S. Long, 2004, **35**, 91-91.
24. A. K. Singh, N. Yasri, K. Karan and E. P. L. Roberts, *ACS Appl. Energy Mater.*, 2019, **2**, 2324-2336.
25. A. K. Sundramoorthy and S. Gunasekaran, 2015, **27**, 1811-1816.

26. H. Liu, Y. Liu and D. Zhu, *J. Mater. Chem.*, 2011, **21**, 3335-3345.
27. M. L. Baker, M. W. Mara, J. J. Yan, K. O. Hodgson, B. Hedman and E. I. J. C. c. r. Solomon, *Coord. Chem. Rev.*, 2017, **345**, 182-208.
28. C. S. Diercks, S. Lin, N. Kornienko, E. A. Kapustin, E. M. Nichols, C. Zhu, Y. Zhao, C. J. Chang and O. M. J. J. o. t. A. C. S. Yaghi, *JACS*, 2018, **140**, 1116-1122.
29. C. Fierro, A. B. Anderson and D. J. T. J. o. P. C. Scherson, *J. Phys. Chem.*, 1988, **92**, 6902-6907.
30. K. M. Carsch, I. M. DiMucci, D. A. Iovan, A. Li, S.-L. Zheng, C. J. Titus, S. J. Lee, K. D. Irwin, D. Nordlund, K. M. Lancaster and T. A. Betley, 2019, **365**, 1138-1143.
31. J. Wang, J. Zhou, Y. Hu and T. Regier, *Energy Environ. Sci.*, 2013, **6**, 926-934.
32. D. Deng, X. Chen, L. Yu, X. Wu, Q. Liu, Y. Liu, H. Yang, H. Tian, Y. Hu, P. Du, R. Si, J. Wang, X. Cui, H. Li, J. Xiao, T. Xu, J. Deng, F. Yang, P. N. Duchesne, P. Zhang, J. Zhou, L. Sun, J. Li, X. Pan and X. Bao, *Sci. Adv.*, 2015, **1**, e1500462.
33. K. Jiang, S. Siahrostami, T. Zheng, Y. Hu, S. Hwang, E. Stavitski, Y. Peng, J. Dynes, M. Gangisetty, D. Su, K. Attenkofer and H. Wang, *Energy Environ. Sci.*, 2018, **11**, 893-903.
34. A. Gorski, A. Starukhin, S. Stavrov, S. Gawinkowski and J. Waluk, *Spectrochim. Acta A Mol. Biomol. Spectrosc.*, 2017, **173**, 350-355.
35. D. R. Roy, E. V. Shah and S. Mondal Roy, *Spectrochim. Acta A Mol. Biomol. Spectrosc.*, 2018, **190**, 121-128.
36. M. Aydin and D. L. Akins, in *Applications of Molecular Spectroscopy to Current Research in the Chemical and Biological Sciences*, BoD–Books on Demand, 2016, p. 141.
37. K. A. Macor and T. G. Spiro, *JACS*, 1983, **105**, 5601-5607.
38. B. Duong, R. Arechabaleta and N. J. Tao, *J. Electroanal. Chem.*, 1998, **447**, 63-69.
39. S. R. Snyder and H. S. White, *J. Phys. Chem.*, 1995, **99**, 5626-5632.
40. J. Choi, P. Wagner, S. Gambhir, R. Jalili, D. R. MacFarlane, G. G. Wallace and D. L. Officer, *ACS Energy Lett.*, 2019, **4**, 666-672.
41. P. Jiang, D. Prendergast, F. Borondics, S. Porsgaard, L. Giovanetti, E. Pach, J. Newberg, H. Bluhm, F. Besenbacher and M. Salmeron, 2013, **138**, 024704.
42. Z. Wang, J. Bentley and N. J. M. Evans, 2000, **31**, 355-362.
43. P. Zhang, L. Li, D. Nordlund, H. Chen, L. Fan, B. Zhang, X. Sheng, Q. Daniel and L. Sun, *Nat. Commun.*, 2018, **9**, 381.
44. P. A. Liddell, M. Gervaldo, J. W. Bridgewater, A. E. Keirstead, S. Lin, T. A. Moore, A. L. Moore and D. Gust, *Chemistry of Materials*, 2008, **20**, 135-142.
45. N. Kornienko, Y. Zhao, C. S. Kley, C. Zhu, D. Kim, S. Lin, C. J. Chang, O. M. Yaghi and P. Yang, *JACS*, 2015, **137**, 14129-14135.